Biomedicine & Pharmacotherapy 133 (2021) 111059

Contents lists available at ScienceDirect

Biomedicine & Pharmacotherapy

journal homepage: www.elsevier.com/locate/biopha

Original article

Paclitaxel antitumor effect improvement in lung cancer and prevention of the painful neuropathy using large pegylated cationic liposomes

Julia Jiménez-López [a,b,c,1], Inmaculada Bravo-Caparrós [c,1], Laura Cabeza [a,b,c], Francisco R. Nieto [d], Raúl Ortiz [a,b,c], Gloria Perazzoli [a,b], Eduardo Fernández-Segura [e], Francisco J. Cañizares [e], José M. Baeyens [d], Consolación Melguizo [a,b,c,*], José Prados [a,b,c]

[a] Institute of Biopathology and Regenerative Medicine (IBIMER), Center of Biomedical Research (CIBM), University of Granada, 18100, Granada, Spain
[b] Instituto Biosanitario de Granada (ibs. GRANADA), 18014, Granada, Spain
[c] Department of Anatomy and Embryology, Faculty of Medicine, University of Granada, 18012, Granada, Spain
[d] Department of Pharmacology, Institute of Neuroscience, Biomedical Research Center (CIBM), University of Granada, 18100, Granada, Spain
[e] Department of Histology, Institute of Neuroscience, Biomedical Research Center (CIBM), University of Granada, 18100, Granada, Spain

ARTICLE INFO

Keywords:
Lung cancer
Paclitaxel
Pegylated liposomes
Peripheral neurotoxicity
Dorsal root ganglia

ABSTRACT

Paclitaxel (PTX), a drug widely used in lung cancer, has serious limitations including the development of peripheral neurotoxicity, which may lead to treatment discontinuation and therapy failure. The transport of PTX in large cationic liposomes could avoid this undesirable effect, improving the patient's prognosis. PTX was encapsulated in cationic liposomes with two different sizes, MLV (180−200 nm) and SUV (80−100 nm). In both cases, excellent biocompatibility and improved internalization and antitumor effect of PTX were observed in human and mice lung cancer cells in culture, multicellular spheroids and cancer stem cells (CSCs). In addition, both MLV and SUV with a polyethylene glycol (PEG) shell, induced a greater tumor volume reduction than PTX (56.4 % and 57.1 % *vs.* 36.7 %, respectively) in mice. Interestingly, MLV-PEG-PTX did not induce either mechanical or heat hypersensitivity whereas SUV-PEG-PTX produced a similar response to free PTX. Analysis of PTX distribution showed a very low concentration of the drug in the dorsal root ganglia (DRG) with MLV-PEG-PTX, but not with SUV-PEG-PTX or free PTX. These results support the hypothesis that PTX induces peripheral neuropathy by penetrating the endothelial fenestrations of the DRG (80−100 nm, measured in mice). In conclusion, our larger liposomes (MLV-PEG-PTX) not only showed biocompatibility, antitumor activity against CSCs, and *in vitro* and *in vivo* antitumor effect that improved PTX free activity, but also protected from PTX-induced painful peripheral neuropathy. These advantages could be used as a new strategy of lung cancer chemotherapy to increase the PTX activity and reduce its side effects.

1. Introduction

Lung cancer is the most common and lethal cancer worldwide, being responsible for one out of every five cancer-related deaths [1]. Its high incidence and poor response to treatment, especially in advanced stages where the disease is usually disseminated, make it necessary to improve existing therapies [2,3]. Currently, non-resectable and/or metastatic lung cancer is treated using platinum and etoposide as first-line treatment. Topotecan and anthracyclines are usually applied as second-line therapies [4], but paclitaxel (PTX) and docetaxel are being increasingly used to improve patient response and prognosis [5–7]. PTX, a diterpene that stabilizes microtubule polymerization by binding to β-tubulin, blocks cells in the G_2/M phase of the cell cycle, leading to cell apoptosis [8–10]. However, this drug has significant limitations that may hinder patient recovery, including the development of resistance by tumor cells or low specificity for tumor tissues. Moreover, PTX can cause undesirable side effects such as reversible alopecia, myelosuppression, arthralgia/myalgia, gastrointestinal effects, asthenia, hypersensitivity reactions or peripheral neurotoxicity (one of the main limitations associated with PTX treatment) [8,11].

In this context, PTX vehiculization using lipid-based nanoformulations represents a potential strategy to overcome the above-

* Corresponding author at: Institute of Biopathology and Regenerative Medicine (IBIMER), Center of Biomedical Research (CIBM), University of Granada, Spain.
E-mail address: melguizo@ugr.es (C. Melguizo).
[1] These authors contributed equally to this work.

https://doi.org/10.1016/j.biopha.2020.111059
Received 11 August 2020; Received in revised form 18 November 2020; Accepted 20 November 2020
Available online 9 December 2020

mentioned limitations and improve its effectiveness. These formulations enhance the bioavailability of drugs by preventing their degradation and elimination in the body, and also increase drug internalization and reduce the development of resistance in tumor cells [12,13]. Resistance to PTX has been overcome with the use of liposomes that allow its direct release into the mitochondria, causing apoptosis in resistant cells. For instance, the use of liposomes led to an 86 % reduction in tumor volume in mice bearing PTX-resistant tumors [14].

In recent years, several lipid formulations have been developed and approved for clinical use (*e.g.* Doxil®, Myocet® and Lipo-DOX®), and others are currently undergoing different phases of clinical trials (*e.g.* Lipusu®, NCT02996214), which proves their therapeutic potential. However, these nanoformulations showed a similar or even higher incidence of undesirable side effects in comparison with free PTX, particularly peripheral sensory neuropathy [15]. Therefore, novel approaches for the development of alternative formulations for PTX are needed to overcome the limitations of current liposomes. Cationic liposomes showed an enhanced ability to be incorporated into the cells by endocytosis, and their pegylation prolonged the circulation times of nanovesicles, avoiding capture by the reticuloendothelial system (RES) [16,17]. The first aim of this study was to assess the *in vitro* and *in vivo* biocompatibility and the antitumor effect of PTX encapsulated in commercial cationic liposomes formulated without and with polyethylene glycol (Lipo-Cat-PTX and Lipo-Cat-PEG-PTX, respectively). Experiments were conducted using two lung cancer cell lines (A549 and LL2) and one non-tumor lung cell line (L132). Moreover, different variables of these liposomes were evaluated, including their effect on the cell cycle profile, their intracellular pharmacokinetics *in vitro* and their biodistribution *in vivo*.

As previously mentioned, one of the most frequent and limiting side effects of PTX is peripheral neurotoxicity, which can lead to the development of painful peripheral neuropathies [18]. Patients treated with PTX report sensory symptoms such as paresthesia, dysesthesia, numbness, electric shock-like sensation and neuropathic pain in a stocking-glove distribution. These symptoms significantly compromise the quality of life of patients and may lead to a dose reduction or even chemotherapy suppression [19,20]. Although much effort has been made at the preclinical and clinical levels, no effective therapies are currently available to treat or prevent this peripheral neuropathy [21]. The pathogenesis of PTX-induced neuropathy has been only partially elucidated [22]. For instance, the concentration of PTX is known to be higher in the dorsal root ganglia (DRG) than in the rest of the nervous system, which is protected by the blood-brain barrier [23–26]. The accumulation of PTX in the DRG, which contain the somas of the peripheral sensory neurons [27], can be explained by the presence of endothelial fenestrations (EFs) in the rich network of capillaries that vascularize the DRG [28]. The second aim of this work was to measure the size of the EFs in the DRG and to vehiculate PTX in cationic liposomes of different sizes in order to modulate its pass through the EFs. Hypothetically, this would reduce the incidence of painful neuropathies without affecting -or even improving- the antitumor activity of PTX.

The results presented in this work show that both PTX nanoformulations were able to improve the pharmacological properties of PTX without the need to use solvents such as Cremophor® EL. In fact, a significant increase in both the *in vitro* and *in vivo* antitumor activity of PTX was observed in lung cancer models with these nanoformulations. Interestingly, the use of MLV-PEG-PTX did not induce peripheral neuropathy in mice whereas SUV-PEG-PTX produced a response similar to that of free PTX. These findings could be explained by the inability of large liposomes to pass through the EFs of the DRG, subsequently preventing PTX from reaching the DRG. Thus, these nanoformulations, and more specifically MLV-PEG-PTX, represent a new therapeutic option for the treatment of lung cancer that may improve the antitumor efficacy of PTX and prevent the development of painful peripheral neuropathy, which is one of its main side effects.

2. Materials and methods

2.1. Materials

Pegylated and non-pegylated cationic liposomes were obtained using the ready-to-use formulations Pronanosome Lipo-Cat-PEG phosphatidylcholine, cholesterol, stearylamine and DSPE-PEG2000 (P90:CHO: Stearylamine:PEG, 1:1:0.18:0.11 M ratio) and Lipo-Cat (P90:CHO: Stearylamine:, 1:1:0.18 M ratio), respectively (Nanovex Biotechnologies, Spain). Liposomes were prepared at a concentration of 70 mg/mL. PTX was obtained from LC Laboratories (Woburn, MA, USA) and was dissolved in a solution of 50 % Cremophor® EL (Sigma-Aldrich, Madrid, Spain) and 50 % absolute ethanol (Scharlau, Barcelona, Spain).

2.2. Synthesis and characterization of liposomes

Precise amounts of PTX and Pronanosome Lipo-Cat or Pronanosome Lipo-Cat-PEG were dissolved using chloroform to obtain PTX-loaded liposomes. Then, the chloroform was removed under reduced pressure in a rotary evaporator (Heidolph Hei-VAP Precision) (Heidolph, Germany). The dried film was hydrated for 45 min at 60 °C using a buffer composed by KCl (1.35 mM), NaCl (68.50 mM), KH_2PO_4 (0.75 mM) and Na_2HPO_4. Finally, the sample was homogenized (SilentCrusher Homogenizer, Heidolph, Germany) at 11,000 rpm for 8 min to obtain MultiLamellar Vesicles (MLV) cationic liposomes. A part of the sample was separated to obtain Small Unilamellar Vesicles (SUV) from MLV using a 750 W sonicator (Sonics, USA) for 10 s (pulsed sonication 1:1, 20 % amplitude). All samples were filtered with filters $<$0.45 μm.

The size of the liposomes and the polydispersity index (PDI) of the sample were determined *via* dynamic light scattering (DSL) using a Zetasizer Nano ZS90 (Malvern Instruments Ltd., UK). Three independent samples were taken from each formulation, and measurements were performed three times for each sample at room temperature (RT) with a 1:100 dilution. The Z-potential of the liposomes was determined by Mixed Mode Measurement-Phase Analysis Light Scattering (M3-PALS) also using a Zetasizer Nano ZS90. In addition, the particles were observed by transmission electron microscopy (TEM) (LIBRA 120 PLUS de CARL Zeiss SMT, Oberkochem, Germany) using diluted dispersions ($\approx$ 0.1 %, w/v) and placing drops on copper grids with formvar film. The grids were then dried at 25.0 $\pm$ 0.5 °C in a convection oven. In order to determine the entrapment efficiency of PTX in liposomes, the entrapped PTX was removed by centrifugation and dialysis. A gentle centrifugation at 4000 rpm for 20 min was carried out prior to dialysis purification. Then, a 2 mL sample was placed into a SnakeSkin dialysis tubing (10k MWCO) (ThermoFisher, USA), immersed in 1000 mL of deionized water at RT, and stirred at 500 rpm for 6 h. Dialyzed and non-dialyzed samples were diluted 1:25 (v/v) with methanol to facilitate rupture of the vesicle membranes and to extract PTX from liposomes. Then, PTX was analyzed by chromatography (RP-HPLC) (Shimadzu, Japan).

2.3. Hemolysis assay

Erythrocytes from human blood (25 mL) (healthy donors from the Andalusian Public Health System Biobank) were obtained following our protocol [29]. The erythrocytes were then diluted (1:50), and 190 μL of the resulting solution (pH 7.4) were added to each well of a V-bottomed 96-well plate. Unloaded liposomes were also added in a volume of 10 μL per well. Positive and negative controls were 20 % Triton X-100 (10 μL) and phosphate buffer (PB), pH 7.4 (10 μL), respectively, also processed following our protocol [29]. The percentage of hemoglobin released from the erythrocytes was determined with a Titertekmultiscan colorimeter (492 nm) (Flow, Irvine, California) using the formula:

$$Hemolysis\ (\%) = \frac{abs.\ of\ the\ sample - abs.\ of\ the\ negative\ control}{abs.\ of\ the\ positive\ control} x\ 100$$

Optical microscopy images of the erythrocytes treated with the different formulations were taken at the highest dose used (500 μg / ml) to analyze morphological modifications.

2.4. Cell culture

The human lung adenocarcinoma cell line A549and the murine lung carcinoma cell line LL2 were purchased from the American Type Culture Collection (Rockville, MD, USA). The non-cancer lung cell line L132 was obtained by the Instrumentation Service Center (CIC, University of Granada, Spain). All cell lines were grown in Dulbecco's Modified Eagle's Medium (DMEM) (Sigma-Aldrich, Madrid, Spain) supplemented with 10 % heat-inactivated fetal bovine serum (FBS) (Gibco, Madrid, Spain) and 1 % penicillin and streptomycin antibiotics mixture, and maintained in an incubator at 37 °C and 5 % CO_2 humidified atmosphere.

2.5. In vitro cytotoxicity assays

Cells were seeded at densities of 5.5×10^3 cells/well in A549, 2.5×10^3 cells/well in LL2, and 8×10^3 cells/well in L132 in 24-well plates with DMEM, incubated overnight at 37 °C, and treated with increasing concentrations (0.1–55 nM) of free PTX and PTX-loaded and unloaded liposomes for 96 h, with renewal of culture medium and drugs at 48 h. A sulforhodamine B (SRB) assay was carried out following our procolol [29]. Finally, the optical density (OD) at 492 nm was measured in a spectrophotometer EX-Thermo Multiskan. Cell survival (%) was calculated according to the following equation:

$$Cell\ survival\ (\%) = \frac{Treated\ cells\ OD - blank}{Control\ OD - blank}\ x\ 100$$

In addition, the IC_{50} was calculated (GraphPad Prism 6 Software, La Jolla, CA, USA) and a measure of improvement between two treatments, the therapeutic index (TI), was determined according to the following equation:

$$TI\ (therapeutic\ index) = \frac{IC_{50} PTX}{IC_{50}\ NPs - PTX}$$

2.6. Intracellular pharmacokinetics

The cells (A549, L132 and LL2) were seeded in 6-well plates (4×10^5 cells/well) in DMEM to determine PTX incorporation using a modification of the protocol described by Li et al. [30]. Then, they were exposed to different treatments (free PTX and PTX-loaded liposomes) at 500 nM for 0.5, 1, 2, 4 and 6 h. After two PBS washes, cells were incubated for 5 min in a lysis buffer composed by 0.1 M Tris-HCl pH 7.5, 0.1 M EDTA pH 8, 0.5 % SDS and 0.1 M NaCl (800 μL), and sonicated for 5 min to facilitate their complete disruption and extraction of intracellular PTX. Methyl tert-butyl ether (MTBE) (500 μL) and an internal standard (docetaxel) (15 μL) were added to the samples which were incubated for 5 min (vortex agitation) and centrifuged at 16,000xg for 5 min. The organic phase (with PTX) was collected and evaporated as described by Fernández-Peralbo et al. [31] for ultraperformance liquid chromatography analysis (WatersT, Acquity H Class model) coupled to a triple quadrupole mass spectrometer (Waterrs, XEVO TQ-S model) (UPLC-MS/MS).

2.7. Flow cytometry cell cycle analysis

All cell lines were seeded in 6-well plates at a density of 6×10^4 cells per well. After 24 h, the culture medium was removed and a free-serum culture medium was added to arrest the cell cycle. The culture medium was changed to DMEM with serum and the treatments (free PTX and formulations of liposomes unloaded and loaded with PTX) were administered after 24 h using the IC_{50} of PTX of each cell line. After 48 h, cells were fixed (70 % ethanol in agitation) at 4 °C (1 h) and washed (twice) with PBS. The pellets were processed using the PI/RNASE Solution Kit (Inmunostep, Spain). Samples were analyzed with a FACScan flow cytometer (Becton Dickinson, San Jose, USA) using FlowJo software.

2.8. Alpha-tubulin immunofluorescence assays

Cells were seeded in 24-well plates at a density of 2×10^4 cells per well in A549 and LL2 and 3×10^4 cells per well in L132. For the cell cycle assay, synchronization of cell cycles was induced using medium without serum for 24 h after cell adhesion. Then, culture medium with serum was renewed and drug treatments were administered at the highest dose used in the cell proliferation assay. After 24 h, cells were fixed (cold 70 % methanol) for 30 min at -20 °C, permeabilized (0.1 % Triton X-100) and blocked with a goat serum solution for 60 min. Then, they were incubated with the primary anti-α-tubulin antibody 1:300 (v/v) (Sigma Aldrich, Spain) (one hour at RT), washed (three times) with PBS-0.1 % Tween, and incubated with an Alexa-Fluor 488-conjugated secondary antibody 1:500 (v/v) (Cell Signaling Technologies, Spain) for 60 min at RT in the dark. Hoechst dye (1:2000) was used to stain the nuclei. The cells were observed by fluorescence microscopy (Leica Microsystems, Wetzlar, Germany).

2.9. Multicellular tumor spheroids (MTS) assays

MTS assays were performed following a modification of the protocol described by Prados et al. [32]. First, 50 μL of agar (1 %) was added in 96-well flat bottom plates. After solidification (30 min), 250 and 400 cells/well of A549 and LL2, respectively, were seeded. Plates were centrifuged at 1,000×g for 10 min to induce MTS formation. After 96 h, MTS were exposed to the treatments (free PTX and PTX-loaded and unloaded liposomes) at the IC_{50} (11.1 nM to A549 and 27.6 nM to LL2). Untreated MTS were used as negative control. MTS growth was monitored every 2–3 days with optical microscopy images, and the largest and smallest diameter (LD and SD, respectively) were measured using ImageJ software (National Institute of Health, USA) to determine the spheroid volume (V, μm^3) with the formula:

$$V = \frac{LD^* SD^{2*} \pi}{6}$$

In addition, a TUNEL assay was performed to determine MTS apoptosis. After exposure to the treatments (96 h), in a similar manner as described above, MTS were fixed with 4% paraformaldehyde (3 h) and processed according to the instructions of the TUNEL kit manufacturer (Roche, Mannheim, Germany). Cell nuclei were counterstained with Hoechst (1:2000) and fluorescence images were captured using confocal microscopy (Nikon A1, Nikon Corporation, Tokyo, Japan).

2.10. Cancer stem cells characterization and proliferation assays

A549 cancer stem cells (CSCs) were isolated and characterized following the method described by Leiva et al. [29]. Accordingly, A549 cells were seeded in 6-well plates (1×10^5 cells/well) pre-coated with 1 % agarose (w/v). After 14 days in the presence of induction medium supplemented with hormone mixture B27, growth factors (EGF, bFGF) and heparin, RNA extraction was carried out (RNeasy Mini Kit, Qiagen, MD, EEUU) to analyze the expression of CSC specific markers (SOX2, OCT4, Nanog, CD133 and HPRT housekeeping gene) by Real-Time PCR (Supplementary Table S1) [33]. For proliferation assays, CSCs were disaggregated with Trypsin/EDTA (1:2), seeded into 96-well plates (1×10^3 cells/well) and treated (free PTX and PTX-loaded liposomes) with a concentration range of 1–100 nM of PTX for 72 h. Cell viability was determined by adding 10 μL of Cell Counting Kit-8 (Dojindo Laboratories, Kumamoto, Japan) to each well for 4 h at 37 °C. Absorbance at 450 nm was measured with a Titertek Multiskan colorimeter (Flow).

Cell survival (%) was calculated as described in Section 2.5.

2.11. In vivo tumor growth inhibition and survival analysis

All the animals used in this work were housed in colony cages with free access to water and food prior to the experiments. The animals were kept in rooms with controlled light and temperature (22 ± 2 °C, and 12 h light-dark cycle) and the behavioral experiments were conducted during the light phase (from 8:00 a.m. to 3:00 p.m.). Animal care was in accordance with institutional (Research Ethics Committee of the University of Granada, Spain; 24102019/177) and international standards (European Communities Council Directive 2010/63).

Immunocompetent female C57BL/6 mice (20−25 g) (Charles River, Barcelona, Spain) were injected subcutaneously on the right flank with 5×10^5 LL2 cells resuspended in 100 μL of PBS (day 0). When the tumors were palpable, the animals were randomly divided into 6 groups of 12 mice (n = 12) and treated intravenously (vein of the tail) with free PTX, Cremophor® EL (vehicle of PTX), MLV-PEG and SUV-PEG (blank liposomes), and MLV-PEG-PTX and SUV-PEG-PTX. One group was treated with saline solution (negative control). The treatment (10 mg/kg of PTX) was applied every three days for a total of four doses. Furthermore, every three days the weight of the mice was monitored and dimensions of the tumor were measured with a digital caliper. The tumor volume (V, mm^3) was calculated using the LD and SD with the formula (4) (see above). The end point of the experiment, when the animals were sacrificed, was day 39 from the day of cell inoculation.

2.12. In vivo assay of PTX biodistribution

Lung tumor-bearing C57BL/6 mice were induced from LL2 cells as described above. When the tumors reached approximately 200 mm^3, the animals were randomly divided into 3 groups of 20 mice. Each group was treated intravenously with free PTX, MLV-PEG-PTX and SUV-PEG-PTX (10 mg/kg of PTX). Four mice from each group were sacrificed at 0.5, 1, 6, 12 and 24 h, and blood and tissue samples (brain, lung, heart, liver, spleen, kidneys, tumor and 6 DRG of the lumbar vertebrae) were collected, weighed and resuspended in a 0.9 % NaCl solution (volume equal to twice the weight) [31]. Then, the samples (except DRG and blood) were homogenized (high-speed homogenizer IKA T10 Basic ULTRA-TURRAX, Germany). The DRG were sonicated in 200 μL of 0.9 % NaCl solution for 5 min in cycles of 30 s. Blood samples were collected in tubes with EDTA and plasma was collected after centrifugation at 1200 *g* for 12 min. Then, samples of each tissue, DRG and plasma (200 μL) were incubated for 5 min in an ultrasonic bath and MTBE (500 μL) and docetaxel (15 μL) were added (final concentration of 150 ng/mL). Each sample was vortexed for 1 min, incubated for 5 min at RT and then vortexed again for 5 min to favor the extraction of PTX. After centrifugation at 16,000 *g* for 5 min, the supernatant was collected and the samples were evaporated under vacuum for analysis by ultra-performance liquid chromatography (UPLC-MS/MS) as described above. The results were expressed in graphs in ng PTX/g tissue and ng PTX/mL in the case of plasma, and in ng PTX/6 in the case of DRG.

2.13. Animal model of paclitaxel-induced painful neuropathy

Experiments were performed on female CD-1 mice (Charles River, Barcelona, Spain) weighing 26−32 g each. Free PTX solution was diluted in sterile physiological saline (NaCl 0.9 %) to a final concentration of 1.4 mg/mL just before administration. The vehicle for free PTX was diluted at the time of injection with saline in the same proportion as the free PTX solution. In addition, PEG-liposomes (SUV-PEG-PTX and MLV-PEG-PTX) with the same PTX concentration (1.4 mg/mL) as the free-PTX solution (the liposomes were not diluted) were tested. Mice were anesthetized with 2 % isoflurane (IsoVet®, B. Braun, Barcelona, Spain), and free PTX (7 mg/kg), PTX vehicle, SUV-PEG-PTX (7 mg/kg), MLV-PEG-PTX (7 mg/kg) and both unloaded liposomes (SUV-PEG and MLV-PEG) were administered intravenously (i.v.) once per day for 5 consecutive days (the cumulative dose of PTX was 35 mg/kg in free PTX and both PTX-loaded liposomes). The day of the first administration is considered day 0. To elucidate the time course of PTX-induced pain hypersensitivity in mice, behavioral responses were tested before the treatment (baseline) and on days 3, 7, 10, 14 and 17 after the first PTX administration (n = 8–13 mice/group). Each mouse was evaluated by means of two nociceptive tests to study the development of mechanical allodynia and heat hyperalgesia induced by PTX. All behavioral evaluations were recorded by a treatment-blinded observer.

2.14. Pain behavioral tests

Mechanical allodynia was assessed using von Frey filaments according to the "up-down" method, with slight modifications [34]. On each day of evaluation, the mice were habituated for 120 min in individual transparent plastic boxes (7 × 7 × 13 cm) placed on wire mesh platforms. After the habituation time, filaments were applied to the plantar hind paws, pressed upward to cause a slight bend in the filament for 2–3 seconds. Calibrated von Frey monofilaments (Touch Test Sensory Evaluator Kit; Stoelting, Wood Dale, IL, USA), with bending forces that ranged from 0.02 to 2 g were applied using the up–down paradigm, starting with the 0.6 g filament and allowing 10 s between successive applications. The response to the filament was considered positive if immediate biting/licking, flinching or rapid withdrawal of the stimulated paw was observed. For each consecutive test, if there was a positive response, then a weaker stimulus was used; if there was no response to the filament, then a stronger stimulus was selected. Both hind paws were evaluated separately and mechanical threshold was calculated as the average of both paws in each animal.

Heat hyperalgesia was assessed using the Hargreave's method, as we previously described [35]. Mice were habituated for 120 min in individual Plexiglas chambers (9 × 9 × 22 cm) placed on a glass floor at 30 °C. After habituation, a beam of radiant heat was focused on the plantar surface of the hind paw with a plantar test apparatus (IITC, CA, USA), until the mouse showed a withdrawal response. The latency of the paw withdrawal was measured with a stopwatch. Each mouse was tested three times on each hind paw and the latencies for both paws were averaged for each measurement time. At least 60 s were allowed between consecutive measurements. A cut-off latency time of 20 s was used for each measurement to avoid skin injury and unnecessary suffering to the animals.

2.15. Transmission electron microscopy analysis

CD-1 mice (Charles River, Barcelona, Spain) were anesthetized with isoflurane (IsoVet®, B. Braun, Barcelona, Spain) and perfused intracardially with 20 mL of saline followed by 30 mL of a fresh solution of 2 % glutaraldehyde/1 % paraformaldehyde in 0.1 M PB, pH 7.4, for 15 min. After perfusion, L4 DRG from the mice were dissected and fixed with 2 % glutaraldehyde/1 % paraformaldehyde in 0.1 M PB, pH 7.2 overnight at 4 °C. Afterwards, the fixation samples were transferred to sucrose 10 % in 0.1 M PB for 24 h at 4 °C, and subsequently fixed with 0.1 % osmium tetroxide in 0.1 M PB, pH 7.2, containing 1 % potassium ferrocyanide for 1 h at 4 °C, dehydrated in a graduated series of alcohols and embedded in epoxy resin. Ultrathin sections were stained with uranyl acetate and lead citrate, and analyzed under a Zeiss LEO 906E TEM (Zeiss, Oberkochem, Germany). ImageJ software was used to measure the diameter of pores in the fenestrated capillaries.

2.16. Statistical analysis

All results are expressed as the mean ± standard deviation of three or more replicates. In all *in vitro* experiments, Student's *t*-test and two-way analysis of variance (ANOVA), followed by the Bonferroni test, were used to analyze the significance between two or more groups,

respectively. All *in vivo* results, *i.e.* pain behavioral studies, tumor volume and mouse weight were analyzed by two-way repeated measures analysis of variance (ANOVA), followed by the Bonferroni test. All tests were performed with the Statistical Package for the Social Sciences (SPSS) v. 15.0 software, and differences were considered statistically significant at a p-value <0.05.

3. Results

3.1. Synthesis and characterization of liposomes

Synthesis and characterization of the liposomes was performed by the company Nanovex Biotechnologies (Spain). The liposome size, polydispersity index (PDI) and zeta potential of the pegylated liposomes were analyzed (Table 1). Morphology was also analyzed (Fig. S1). The characterization of the non-pegylated liposomes is included in the supplementary material (Supplementary Table S2).

As intended in the experimental design, the synthesis of nanoformulations with two very different sizes was achieved. MLV-PEG liposomes showed a diameter greater than 180 nm. By contrast, SUV-PEG liposomes showed a diameter lower than 100 nm. PTX-loaded MLV and SUV liposomes showed a PDI around 0.38 (Table S2) while pegylated liposomes were characterized by a PDIs of 0.592 and 0.409 for MLV-PEG-PTX and SUV-PEG-PTX, respectively (Table 1). This range could be due to the presence of PEG in the nanoformulations and by the high concentration of lipids to encapsulate a greater amount of PTX. Finally, both formulations demonstrated a lower positive charge (+1.59 and +3.69 mV for MLV-PEG-PTX and SUV-PEG-PTX, respectively) because of the negative charge of the PEG polymer. Chromatographic analysis indicated a PTX entrapment efficiency greater than 80 % in all liposomes. The amount of PTX per unit mass of lipid in MLV-PTX and SUV-PTX was 22.4 and 20 μg PTX/mg, respectively.

3.2. In vitro hemolysis assay

Pegylated and non-pegylated blank liposome formulations (MLV, SUV, MLV-PEG and SUV-PEG) caused less than 2 % hemolysis. MLV-PEG caused the least rupture of erythrocytes (less than 1 %) at the highest dose. In addition, no morphological changes in erythrocytes were observed after exposure to different liposomes. These results indicate an excellent biocompatibility of the liposomes, which is an essential property for *in vivo* administration (Supplementary Fig. S2).

3.3. Cytotoxicity assays and intracellular pharmacokinetics

MLV-PEG-PTX and SUV-PEG-PTX significantly reduced PTX IC_{50} in the LL2 cancer cell line (1.88 and 2.05-fold, respectively) (Fig. 1A). By contrast, no IC_{50} modulation was detected in the A549 cell line (Table 2). Interestingly, none of the formulations showed a slight increase in toxicity in the L132 cell line in relation to PTX (Table 2). In addition, cellular internalization assays were performed to determine if the improvement of the antitumor effect of the liposome-PTX was related to a greater incorporation of the drug into the cells. Pegylated liposomes (MLV-PEG-PTX and SUV-PEG-PTX) increased intracellular PTX in the first hours of exposure (~2.5-fold) in A549 cells compared to free PTX (Fig. 1B). On the contrary, no significant differences were observed between free PTX and PTX-loaded pegylated formulation in LL2 cells during the first 6 h (Fig. 1B). L132 cells showed a different pattern of PTX incorporation into the lung tumor cell lines, since a higher intracellular concentration of PTX was found after exposure to free PTX compared to PTX-loaded pegylated liposomes (Fig. 1B).

Blank liposomes were not toxic for any of the cell lines tested, which demonstrates their safety and biocompatibility (Supplementary Fig. S3). Results of the cytotoxicity and cellular internalization assays with the non-pegylated formulations are included in the supplementary material (Supplementary Fig. S4 and Table S3).

Table 1
Characterization of liposomes: size, polydispersity index (PDI) and zeta potential of PTX-loaded and unloaded MLV-PEG and SUV-PEG liposomes.

Liposomes	Size (nm)	Polydispersity index (PDI)	Zeta potential (mV)
MLV-PEG-PTX	183 ± 29.1	0.592 ± 0.049	+1.59 ± 0.19
MLV-PEG	186 ± 20	0.500 ± 0.009	+8.71 ± 1.8
SUV-PEG-PTX	88.48 ± 19	0.409 ± 0.006	+3.69 ± 0.52
SUV-PEG	91.37 ± 24	0.408 ± 0.005	+9.48 ± 0.55

Data represent the mean value ± SD of triplicate experience.

3.4. Cell cycle and immunofluorescence analysis

To determine the possible modulation of the mechanism of action of PTX caused by liposomes, we analyzed the cell cycle and alpha-tubulin expression. Cells treated with blank liposomes showed no modulation of the cell cycle profile compared to untreated control cells. By contrast, MLV-PEG-PTX induced a greater accumulation of cells in the $subG_1$ phase in both the A549 and LL2 cell lines compared to those treated with free PTX. However, no cell cycle modifications were observed with SUV-PEG-PTX. Finally, free PTX caused a greater $subG_1$ accumulation and G_2/M arrest than liposome formulations in L132 cells, while PTX-loaded liposomes induced a greater arrest in the S phase (Supplementary Fig. S5). In addition, an immunofluorescence assay using an anti-alpha-tubulin antibody was performed to corroborate that PTX encapsulation in liposomes does not affect G_2/M phase arrest. First, the pattern of alpha-tubulin labeling was similar in the control cells and in the cells treated with blank liposomes in the three cell lines studied (Supplementary Fig. S6). Secondly, the cells treated with PTX and PTX-loaded liposomes showed a very similar labeling, with microtubules condensation in unstructured nuclei of the affected cells. These results suggest that PTX encapsulation does not affect its antimitotic mechanism of action in any of the cell lines. This profile could correspond to an irreversible metaphase arrest causing the stop in phase G_2/M, typical of this antimitotic drug. In some cells with this profile, spindle multipolarization associated with PTX treatment can be observed (Supplementary Fig. S6).

3.5. Multicellular tumor spheroids (MTS) assays

Multicellular tumor spheroids (MTS) from A549 and LL2 cells, an experimental model that mimics tumors *in vivo*, were used to determine the penetrability and antitumor effect of PTX-loaded liposomes. PTX unloaded liposomes did not significantly modify the volume of MTS in either A549 or LL2 cells (Fig. 2A). By contrast, MLV-PEG-PTX significantly reduced A549 MTS volume with respect to untreated MTS, with a 64.3 % decrease at day 8. In addition, this formulation induced a greater decrease in A549 MTS volume compared to free PTX, which only reduced the volume of A549 MTS by 48 % (Fig. 2A). However, treatment with SUV-PEG-PTX did not show MTS volume modulation in comparison to PTX. On the other hand, in LL2 MTS, characterized by a rapid growth (from 0.02 to 0.5 mm^3 at day 8), no significant differences were found with the use of pegylated nanoformulations in comparison to free PTX, which induced a 75 % decrease in MTS volume in relation to the control (Fig. 2A). In view of these results, a TUNEL assay was performed to determine the modulation of MTS apoptosis. The results showed a greater area of apoptotic cells in A549 MTS treated with MLV-PEG-PTX compared to free PTX. In contrast, the smaller formulations (SUV-PEG-PTX) induced an apoptotic labeling in MTS similar to that observed with free PTX (Fig. 2B). On the other hand, analysis of LL2 MTS revealed a similar apoptotic cell labeling with PTX-loaded liposomes and free PTX (Fig. 2B). Untreated MTS and those treated with unloaded liposomes (blank) did not show TUNEL labeling. These results supported the findings related to MTS volume and confirmed the increase in the antitumor effect of PTX when the drug was encapsulated in liposomes.

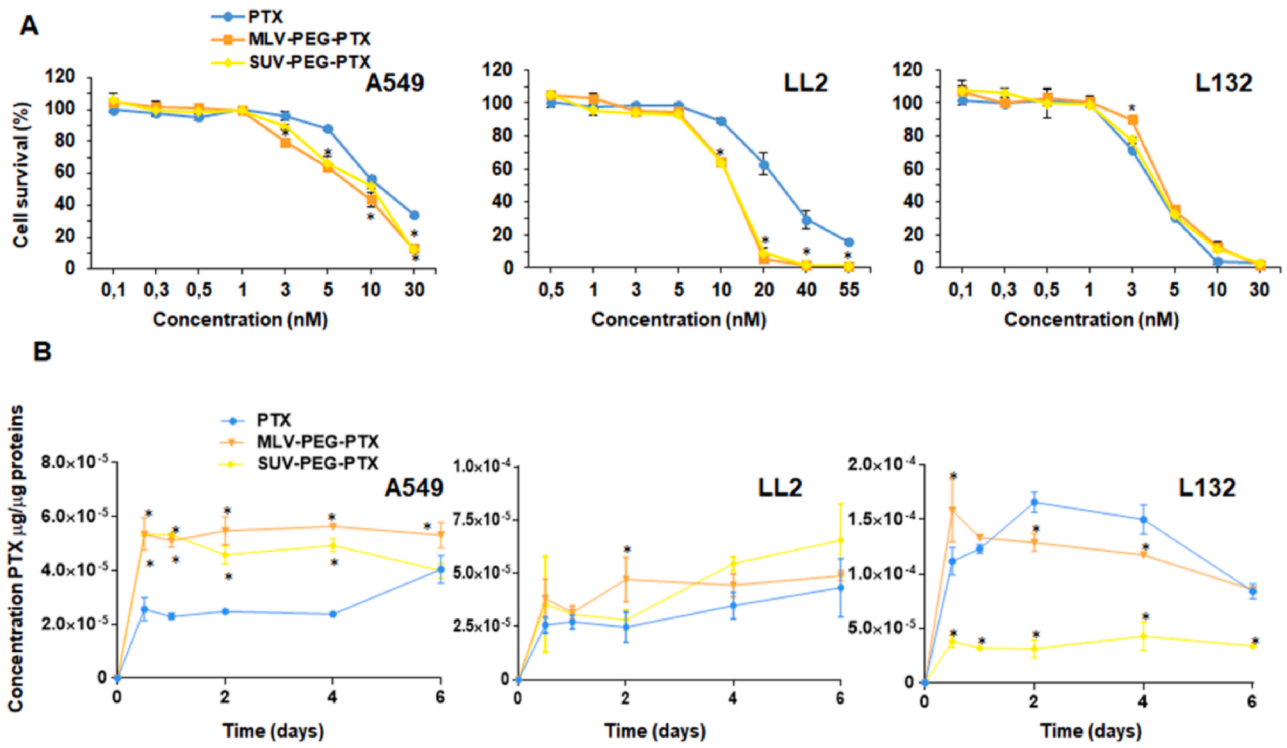

Fig. 1. Proliferation assay and intracellular pharmacokinetics in cell lines using PTX-loaded pegylated liposomes (MLV-PEG-PTX and SUV-PEG-PTX). A. Proliferation assay in lung cancer cell lines A549, LL2 and non-lung tumor cell line L132. Cells were exposed for 4 days to increasing concentration of free PTX or cationic liposomes. Results were represented as % of cell survival. B. Intracellular pharmacokinetics of PTX-loaded liposomes. UPLC-MS/MS was used to determine PTX concentration at different times (0.5, 1, 2, 4 h) in the A549, LL2 and L132 cell lines after exposure to free PTX and PTX-loaded liposomes (500 nM). Data represent the mean value ± SD of triplicate. *Data with significant differences between the treatment with PTX-loaded liposomes and free PTX ($p < 0.05$).

Table 2
Determination of the IC_{50} of lung cell lines exposed to free PTX and pegylated PTX-loaded MLV and SUV nanoformulations.

Cell line	PTX (nM)	MLV-PEG-PTX (nM)	IT	SUV-PEG-PTX (nM)	IT
A549	10.5 ± 0.9	7.7 ± 1	1.36	9,6 ± 2.15	1.09
LL2	27.65 ± 0.8	14.7 ± 3.2	1.88	13.45 ± 1.3	2.05
L132	4.85 ± 1.1	4.23 ± 0.3	1.14	4.5 ± 0.4	1.08

Data represent the mean value ± SD of triplicate experience.

MTS assays with the non-pegylated formulations are included in the supplementary material (Suplementary Fig. S7).

3.6. Cancer stem cells proliferation assay

Tumor spheres from A549 CSCs were observed from day 4 (around 300 µm), and were isolated and characterized (see Methods) using specific markers (Fig. 3A). As shown in Fig. 3B, the concentration of PTX and PTX-loaded liposomes used against CSCs (1–100 nM) did not reach the PTX IC_{50} and the effect of the different treatments was equalized around 65–70 % of cell survival, except in A549 CSCs treated with SUV-PEG-PTX, where survival was not decreased by 80 %. Interestingly, MLV-PEG-PTX showed greater toxicity in CSCs, overcoming the effect of PTX in the range of concentrations between 5–75 nM. By contrast, SUV-PEG-PTX had the lowest antitumor effect on A549 CSCs, specifically with respect to free PTX and MLV-PEG-PTX at 50–100 nM. The CSC proliferation assay with non-pegylated formulations is included in the supplementary material (Suplementary Fig. S8).

3.7. In vivo tumor growth inhibition

C57BL/6 mice with induced subcutaneous lung tumors were treated with free PTX, PTX-loaded liposomes or PTX-unloaded liposomes. Both MLV-PEG-PTX and SUV-PEG-PTX induced a significantly greater tumor volume reduction than free PTX (31.5 % and 32.7 %, respectively), corroborating that PTX encapsulation improved the antitumor drug effect (Fig. 6A). On the other hand, no differences were found in tumor growth between control group and groups treated with blank liposomes (Fig. 4A). In addition, no increase in PTX toxicity was observed with the use of MLV-PEG-PTX and SUV-PEG-PTX, since no significant weight loss was detected in the treated mice compared to the group treated with free PTX (Fig. 4B).

3.8. PTX biodistribution in vivo assays

Fig. 7 shows the study of PTX pharmacokinetics and biodistribution after treatment with free PTX or PTX-loaded pegylated liposomes. The pattern of distribution depends on the time, tissue and type of treatment considered. Free PTX reached higher concentrations in the plasma, heart and kidneys of mice compared to treatment with PTX-loaded liposome at short times (0.5 and 1 h) after administration. During the first 6 h, greater accumulation of MLV-PEG-PTX was observed in the liver, spleen and lungs, with concentrations similar to free PTX. By contrast, SUV-PEG-PTX increased drug bioavailability in comparison with free PTX and MLV-PEG-PTX at longer times (12−24 h) after administration (Fig. 5A). When tissue type is considered, PTX concentration in the heart was lower with MLV-PEG-PTX than with the rest of treatments at all times considered; whereas PTX concentration in the lung was greater with SUV-PEG-PTX than with the rest of treatments at all times considered, except at 0.5 h (Fig. 5A). On the other hand, plasma analysis detected high concentrations of PTX during the first hour after free PTX treatment, but lower concentrations of the drug with the use of MLV-PEG-PTX or SUV-PEG-PTX (Fig. 5B). Interestingly, while the plasma PTX concentration showed a rapid decline 1 h after free PTX administration, SUV-PEG-PTX was able to maintain significantly higher levels of

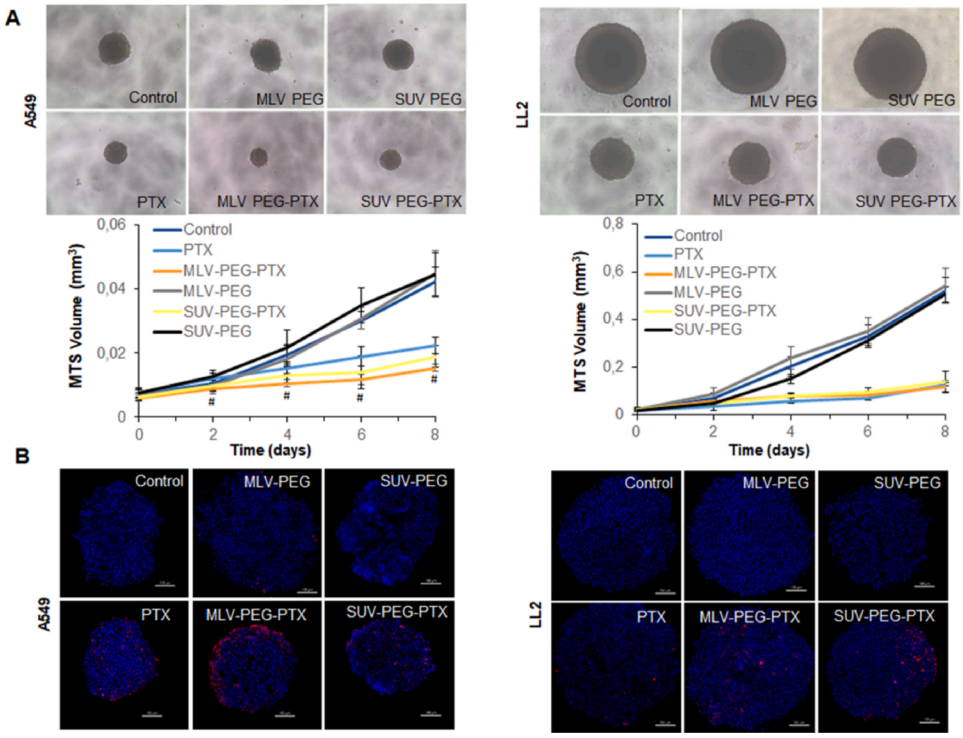

Fig. 2. Multicellular tumor spheroids (MTS) assays. A. Representative images of A549 MTSs and LL2 MTS after treatments (day 8) (magnification, 4X). Graphics represent the monitorization of MTS volume (mm^3). Untreated MTS and MTS treated with the unloaded liposomes were used as control. Data represent the mean value ± SD of 8 replicates. *Data with significant differences between the treatment with SUV-PEG-PTX and free PTX ($p < 0,05$). #Data with significant differences between the treatment with MLV-PEG-PTX and free PTX ($p < 0,05$). B. Analysis of apoptosis by TUNEL assay. Representative fluorescence images of A549 and LL2 MTS untreated (control) and treated with free PTX and different liposomes unloaded and loaded with PTX. Apoptosis (red) induced by exposure for 4 days to the treatments. The nuclei (blue) were stained with Hoechst. Scale bar =100 μm (For interpretation of the references to colour in this figure legend, the reader is referred to the web version of this article).

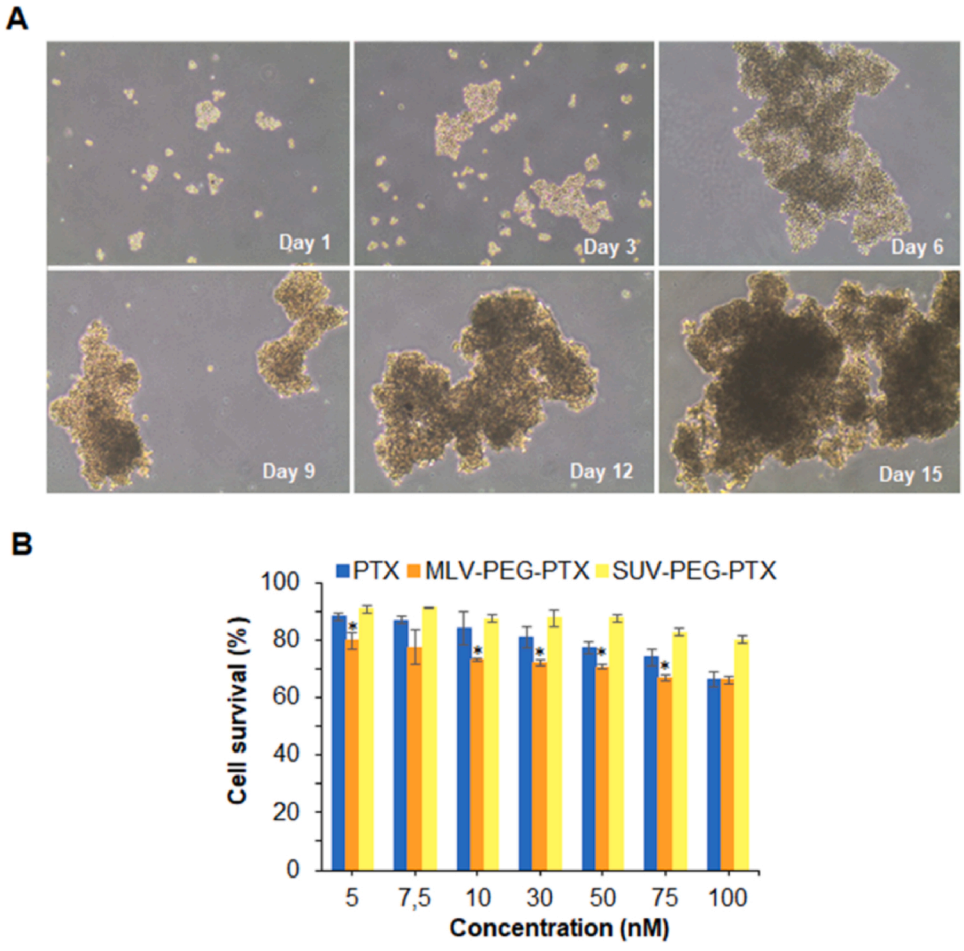

Fig. 3. Isolation and proliferation assays of cancer stem cells (CSCs). A. Representative microscopy images of A549 CSCs isolation (day 1 to 15) with characteristic formation of cellular aggregates (magnification, 4X). B. Proliferation assay of CSCs after exposure (72 h) to free PTX and PTX-loaded liposomes (1–100 nM). Untreated CSCs were used as negative control. Results were represented as % of cell survival. Data represent the mean value ± SD of eight replicates. *Data with significant differences between the treatment with PTX-loaded liposomes and free PTX ($p < 0.05$).

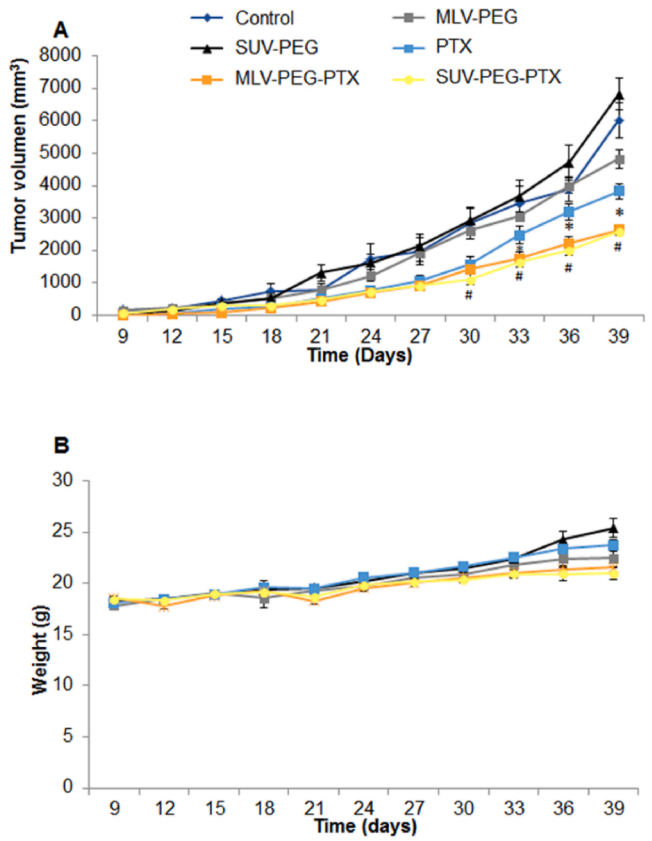

Fig. 4. *In vivo* tumor growth inhibition and mice weight progress. A. Graphic representation of lung tumor volume growth in C57BL/6 mice. Mice were intravenously treated with free PTX and PTX-loaded pegylated liposomes. Untreated mice and mice treated with unloaded liposomes and Cremophor were used as controls. Data are represented as the mean ± S.D. (n = 12). *Significant inhibition of tumor growth comparing MLV-PTX or MLV-PEG-PTX *versus* free PTX ($p < 0.05$). #Data with significant differences between treatment with SUV-PTX or SUV-PEG-PTX and free PTX ($p < 0.05$). B. Graphic representation of the monitorization of mice weight progress. Data are represented as the mean ± S.D. (n = 12).

PTX in the plasma at 6, 12 and 24 h (Fig. 5B). Lumbar DRG tissue was also analyzed. It was observed that, while free PTX and SUV-PEG-PTX treatments induced PTX accumulation, no PTX was detected in these neurological structures after the first hour of MLV-PEG-PTX treatment (Fig. 5C). Finally, when tumor PTX concentration was measured, it was found that free PTX administration yielded a higher concentration than liposomes up to 6 h, whereas SUV-PEG-PTX treatment allowed a greater PTX accumulation in the tumor tissue at 24 h compared to free PTX and MLV-PEG-PTX. (Fig. 5D). This fact could explain that SUV-PEG-PTX treatment induced a greater tumor suppression rate than PTX treatment.

3.9. *In vivo paclitaxel-induced painful neuropathy*

To determine the modulation of paclitaxel-induced painful neuropathy by liposomes, we compared the mechanical- and heat-hypersensitivity induced by 7 mg/kg of PTX administered as SUV-PEG-PTX, MLV-PEG-PTX or free PTX in CD-1 mice. The baseline responses to the von Frey and Hargreave's tests before any treatment were not significantly different between all groups (Fig. 6A and B). Mice injected with free PTX, SUV-PEG and MLV-PEG (control PTX-unloaded liposomes) did not significantly modify post-administration responses in both behavioral tests. However, free PTX induced mechanical allodynia (Fig. 6A) and heat hyperalgesia (Fig. 6B), manifested as a reduction of threshold forces for paw withdrawal following mechanical stimulation, and decreased latencies to paw withdrawal after heat stimulation, respectively. Treatment with SUV-PEG-PTX induced a pattern of development of painful neuropathy similar to that of free PTX; whereas MLV-PEG-PTX did not induce either mechanical (Fig. 6A) or heat hypersensitivity (Fig. 6B), as these mice showed post-administrations responses similar to those treated with MLV-PEG. Therefore, these results show that it is possible to prevent the development of PTX-induced painful neuropathy by modifying the size of the liposome in which this chemotherapeutic is administered.

3.10. *Transmission electron microscopy analysis of capillaries in the DRG*

Fig. 7 illustrates the ultrastructural characteristics of capillaries from L4 DRG, which showed the presence of continuous and fenestrated capillaries. Continuous capillaries were characterized by an uninterrupted endothelium and a continuous basal lamina (Fig. 7A). Fenestrated capillaries in L4 DRG were characterized by an interrupted endothelium with pores measuring 80−100 nm in diameter, and a continuous basal lamina (Fig. 7B and C).

4. Discussion

Paclitaxel (PTX) is a cytotoxic drug with several properties that make it suitable for the treatment of lung cancer. However, it has significant drawbacks including low therapeutic efficiency, drug resistance, poor solubility and, especially, toxicity –*i.e.* neurotoxicity-. The use of excipients such as Cremophor or Tween 80 have facilitated the solubilization of PTX for clinical treatments. Nevertheless, these substances have many drawbacks, including neurotoxicity and hypersensitivity reactions [15,36–39]. In this work, cationic liposomes with different sizes (*i.e.* MLV, >180 nm; and SUV, <100 nm) were combined to PTX in order to improve its pharmacological properties and reduce its side effects. In addition, a PEG coating was incorporated to enhance its properties *in vivo*.

Liposomes have been traditionally considered to have good biocompatibility properties because their design is based on phospholipids generally present in biological membranes. Nevertheless, the modification of chemical groups on the surface of the nanoformulation can influence its hemoreactivity. In fact, commercial liposomes with PEG coatings, such as Doxil®, can cause a hypersensitivity syndrome known as 'complement activation-related pseudoallergy' [40]. Other liposomes, composed of phosphatidylcholine (PC) and phosphatidylinositol (PI) and combined with lipophilic prodrugs, showed hemolysis rates below 1 % [31]. Furthermore, Nie et al. [41] synthesized liposomes with different zeta potentials and observed that liposomes with a PEG coating had less impact on rabbit erythrocytes than non-pegylated liposomes. Conversely, our formulations showed excellent *in vitro* biocompatibility in both tumor and non-tumor lung cell lines and in human erythrocytes, either with or without PEG coating.

Interestingly, PTX encapsulation in both MLV and SUV liposomes significantly enhanced its antitumor effect *in vitro* in comparison with free PTX. Specifically, in the LL2 cell line, a PTX IC_{50} reduction of up to 2 and 5 times was achieved with pegylated and non-pegylated liposomes, respectively. Similar studies using PTX-loaded liposomes against NCI-H460 lung tumor cells showed a less significant IC_{50} increase (less than two-fold) when comparing the lipid formulation (14 nM) with free PTX (21 nM) [42]. Zhang et al. [43] synthesized other liposomes loaded with PTX functionalized with a peptide that favors cellular internalization (PFV-Lip-PTX), with which they obtained greater antitumor efficacy *in vitro* in the MCF-7 breast tumor line compard to liposomes without peptide. These PFV-Lip-PTX liposomes presented an IC_{50} 3.26 times higher than free PTX, although they achieved higher tumor volume reduction *in vivo* compared to free PTX. Likewise, the docetaxel-loaded liposomes synthesized by Hua et al. [44] increased cellular internalization of the drug in the PC-3 cell line. Similar results were observed using PTX-loaded albumin liposomes, which improved drug internalization in the MCF7 and B16F10 cell lines [45]. Cell cycle and

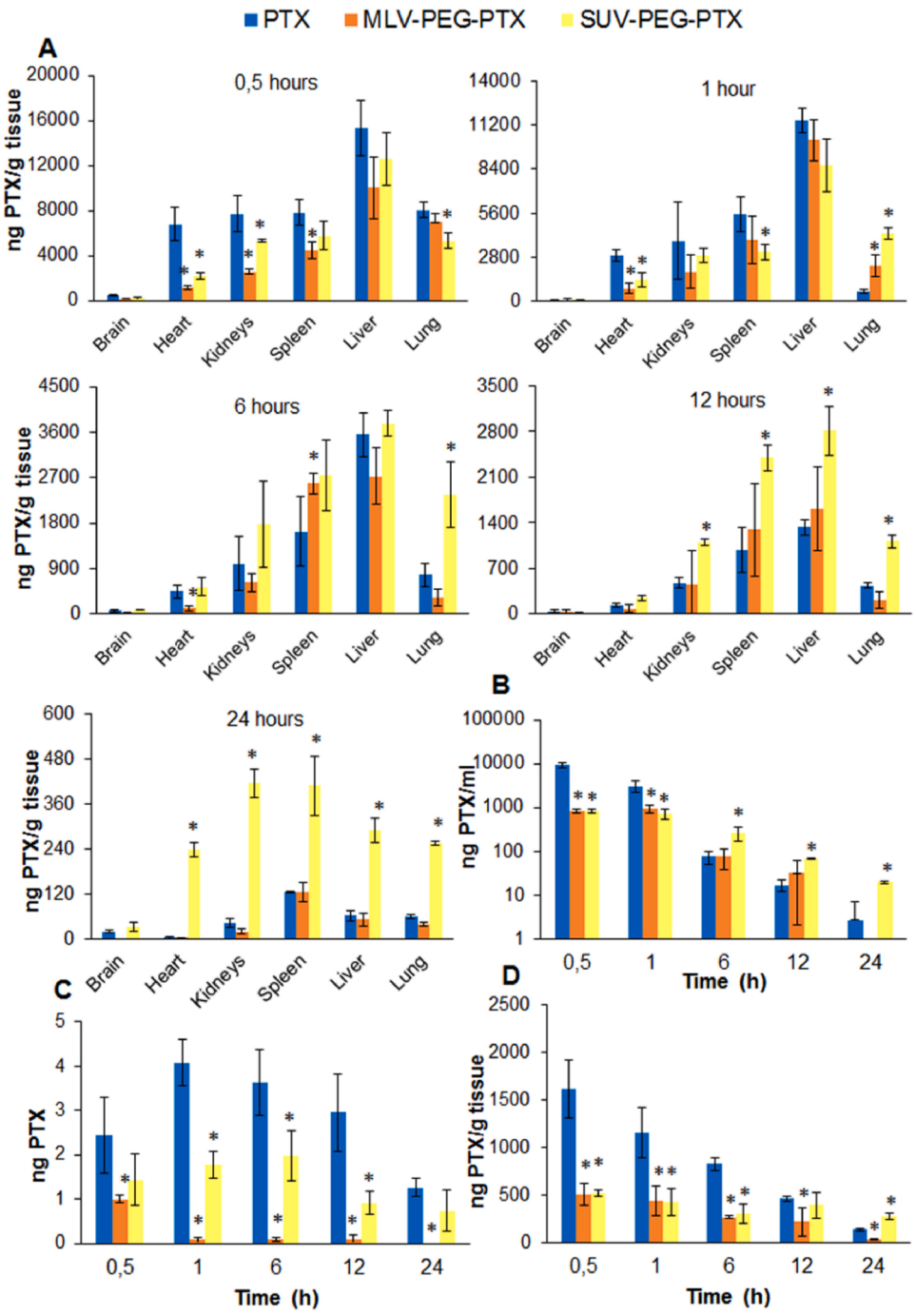

Fig. 5. PTX biodistribution *in vivo* assays. PTX concentration (ng PTX/g tissue) was determinated at 0.5, 1, 6, 12 and 24 h in tissues of mice treated with a single dose of 10 mg/kg of free PTX and PTX-loaded liposomes (MLV-PEG-PTX and SUV-PEG-PTX). The tissues extracted for the determination of PTX were the brain, heart, kidneys, spleen, liver and lungs (A). PTX was specifically quantified in plasma (ng PTX/mL plasma) (B), in the DRG of the lumbar vertebrae (ng PTX) (C) and in the tumor tissue (ng PTX/g tissue) (D) at different times after administration. Results were expressed as the mean value of five replicates ± SD. *Data with significant differences between the treatment with MLV-PEG-PTX or SUV-PEG-PTX and free PTX ($p < 0.05$).

immunofluorescence assays showed that MLV-PTX liposomes increased the SubG1 subpopulation compared to free PTX and induced metaphase arrest subsequently leading to G2/M phase arrest. Similar images of spindle multi-polarization in the nuclei have been described in prostate and breast cancer cells exposed to free PTX or PTX-loaded liposomes [46,47]. In addition, the improved antitumor activity of our liposomes can be explained by the increased internalization of PTX in the tumor cells. Interestingly, the internalization of free PTX in the non-tumor cell line L132 was greater than that of PTX-loaded liposomes, which could suggest a certain intrinsic specificity of the formulations for tumor cells.

In order to analyze the penetrability of liposomes, we performed MTS assays that mimic *in vivo* tumors. Other authors such as Wang et al. [48] added cell-penetrating peptides to liposomes in order to improve their penetrability in tumor spheroids. However, this addition may reduce the biocompatibility and increase the systemic toxicity of the formulations. In accordance with cytotoxicity assays, MLV-PEG-PTX showed the greatest antitumor effect on A549 MTS. However, in LL2 MTS, the non-pegylated liposomes achieved the greatest volume reduction, suggesting that pegylation could reduce PTX internalization. The different morphology and growth of the MTS assayed coul be related to their behaviour in relation to PEG-PTX. In fact, A549 MTS were smaller and less compact than LL2 MTS, enabling a greater penetrability of the formulations, and showed a lower growth rate (size from 0.04 mm^3 in A549 to 0.5 mm3 in LL2 at day 8). Our results are comparable to those obtained by Pereira et al. [49] using PC3 spheroids treated with non-pegylated and pegylated docetaxel-loaded liposomes. Non-pegylated nanoformulations improved the penetration and antitumor effect of the drug after long exposure times (72 and 96 h) in

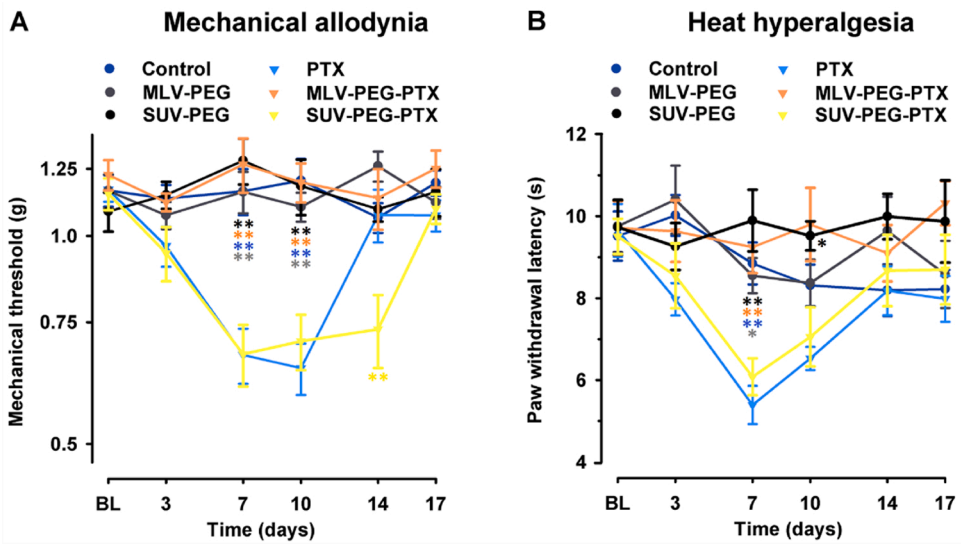

Fig. 6. Time-course of the effects on mechanical and thermal thresholds of mice treated during 5 consecutive days with free PTX (7 mg/kg), PTX vehicle, SUV-PEG-PTX (7 mg/kg), MLV-PEG-PTX (7 mg/kg) and both unloaded liposomes. The von Frey threshold (A) and latency to hind paw withdrawal in the Hargreave's test (B) were recorded 1 day before (BL) and on days 3, 7, 10, 14 and 17 after the first intravenous administration. Each point and vertical line represents the mean ± SEM of the values obtained in 10-12 animals. Statistically significant differences in comparison to free PTX and the other groups of treatment: *$p < 0.05$ and **$p < 0.01$.

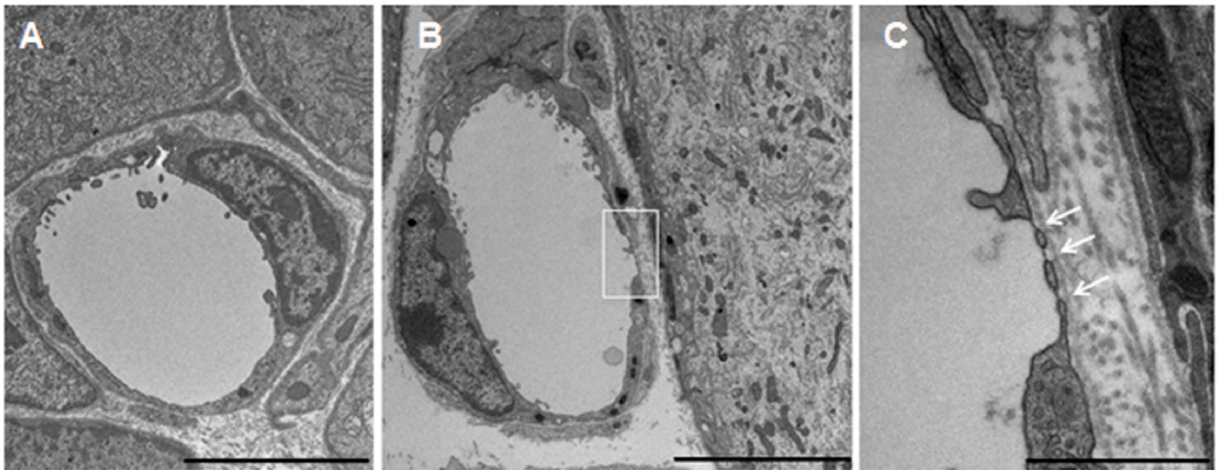

Fig. 7. Transmission electron micrographs of continuous and fenestrated capillaries from L4 DRG of the CD-1 mice. (A) Cross-section of a continuous capillary; (B) Cross-section of a fenestrated capillary (C) High magnification of pores in the fenestrated capillaries which are bridged by a diaphragm (arrows). Scale bar: 5 μm (A, B), and 1 μm (C).

comparison with free docetaxel and pegylated docetaxel-loaded liposomes. A significant reduction of cell viability (30 %) was observed with non-pegylated liposomes as compared to the free drug and pegylated liposomes (60 %).

Prior to performing the cytotoxicity assays on CSCs, these cells were isolated and characterized by their morphology and the expression of specific stem cell markers. The results of this characterization were similar to those reported by various authors [29,33,50–52], which confirmed the CSC phenotype. Once the phenotype of CSCs was verified, the cytotoxicity assay was performed, in which, interestingly, only MLV-PEG-PTX significantly decreased CSCs viability compared to free PTX. Other studies using CSCs (CD133+) from mouse sarcoma showed that treatment with pegylated liposomes loaded with epirubicin and metformin induced a greater antitumor effect than the free drugs [53]. In addition, Füredi et al. [54] showed that treatment with DOX-loaded pegylated liposomes was much more effective in DOX-resistant cells mediated by P-glycoprotein (*i.e.* a typical resistance mechanism in CSCs) than the free drug. The authors hypothesized that the use of liposomes might improve drug pharmacokinetics, requiring higher levels of P-glycoprotein to confer cellular resistance. In this context, our results suggest that larger liposomes could incorporate more PTX molecules which can offset the expulsion of drugs in CSCs through resistance mechanisms such as P-glycoprotein. In addition, MLV-PEG coating could favor evasion of the resistance mechanism of CSCs. Both hypotheses will require further studies to be verified.

Based on the promising *in vitro* results of PTX-loaded MLV and SUV liposomes, an *in vivo* study was conducted in C57BL/6 mice to analyze the biodistribution, pharmacokinetics and antitumor activity of treatments with free PTX, MLV-PEG-PTX and SUV-PEG-PTX. First, the biodistribution results showed that smaller liposomes (SUV-PEG-PTX) increased drug bioavailability in all tissues more than MLV-PEG-PTX, as discussed above, probably because its high size favors a faster systemic elimination through the RES. These results are supported by those obtained by Zhao et al. [55] using PTX-loaded of 500 nm size. These liposomes were administered in dogs, showing a similar biodistribution pattern than free PTX at 2 and 12 h, with a greater drug accumulation in the liver, spleen, and lungs. Similarly, PTX was detected in tumor tissues in large quantities during the first 6 h in the mice treated with free PTX. However, at 24 h, the highest accumulation of PTX was observed with SUV-PEG-PTX liposomes. These results suggest that liposome formulations probably require a longer time in circulation to reach the tumor tissue. This hypothesis is supported by other studies in mice with

induced tumors (leukemia) in which cationic liposomes increased the concentration of the encapsulated drug (doxorubicin) in the tumor tissue at 24 h of treatment compared to the free drug [56]. Even more, some nanoformulations loaded with a fluorophore were not detected in the tumor tissue until 48–72 h after administration [57].

In vivo results showed that both liposomes (MLV-PEG-PTX and SUV-PEG-PTX) significantly reduced tumor growth and volume in comparison with free PTX, mainly in the last days of the experiment (33–39 days). These differences in tumor volume suggest that liposomes remained bioavailable for longer than free PTX and that they required more than 24 h to accumulate in the tumor tissue, as discussed above. Moreover, liposome treatment did not cause toxicity in mice, and a normal pattern of weight gain and growth was observed. Our results overcome those repored by Hua et al. [44] with docetaxel-loaded liposomes, which did not improve the *in vivo* antitumor activity of the drug in mice with PC-3-induced tumors. In addition, similar results were obtainted by Qi et al. [58] and by Yang et al. [59] using PTX-loaded pegylated liposomes in ovarian and breast cancer murine nude models. In both cases, the difference in tumor volume between both free PTX and liposome treatment was observed few days after treatment initiation. In our study, this difference was observed at a longer time. This could be attributed to the charge of the liposome surface since Yang et al. [59] used pegylated liposomes negatively charged, which decrease the RES uptake while increase penetrability. Our cationic pegylated liposomes probably require a longer exposure to penetrate the tumor tissue, supporting the results of the biodistribution assay.

Interestingly, the biodistribution analysis detected a very low PTX concentration in the DRG using large liposomes (*i.e.* MLV-PEG-PTX) in comparison with smaller liposomes (*i.e.* SUV-PEG-PTX) and free PTX. The DRG, where the cell bodies of the peripheral sensory neurons are located, have a rich vasculature [28] with EFs, making them particularly sensitive to neurotoxic agents [60]. In fact, PTX levels in the DRG have been previously associated with sensory neurotoxicity [27,61]. Transmission electron microscopy was used for the first time to measure the size of these EFs in mice, which showed a diameter of 80−100 nm. This observation provides rationale for the hypothesis that PTX encapsulation in liposomes larger than the EFs of the DRG could prevent the entry of PTX into the DRG, subsequently reducing the development of peripheral neuropathy. The administration of MLV-PEG-PTX did not induce either mechanical or heat hypersensitivity in mice whereas SUV-PEG-PTX produced a response similar to free PTX, supporting our hypothesis. Recently, Zang et al. [62] used pegylated liposomes (phosphatidylcholine and cholesterol) loaded with PTX and observed that sensitivity to mechanical and heat stimulation did not increase with respect to free PTX in rats, preventing the development of peripheral neuropathy. The size of the pegylated liposomes (140 ± 13 nm) used in this study was similar to our MLV-PEG-PTX liposomes (183 ± 29.1 nm), supporting our results. Nonetheless, the size of the EFs in the rat DRG vasculature is unknown. According to our hypothesis, liposomes larger than the EFs of the DRG would not be able to enter the DRG and, thus, would not release PTX. Therefore, the neuronal cells therein located would not be damaged, preventing the development of peripheral neuropathy. These results emphasize the importance of MLV liposomes, since no previous studies have investigated the prevention of painful peripheral neuropathy with lipid formulations.

The large size of MLV-PEG-PTX would limit its entry into the DRG, where PTX has been shown to activate TLR4, leading to higher expression of MCP-1 by the DRG neurons. This increased expression would then lead to greater infiltration of the DRG by macrophages expressing inflammatory cytokines, resulting in loss of intraepidermal nerve fibers and eventual development of PTX-induced peripheral neuropathy [63]. Other pegylated liposomes have shown excellent clinical outcomes, as is the case with Doxil®, which transports the chemotherapeutic drug doxorubicin. This liposome formulation has been shown to have a higher antitumor effect and to reduce side effects of doxorubicin such as myelosuppression or cardiotoxicity in recurrent ovarian cancer, metastatic breast cancer and AIDS-related Kaposi's sarcoma [64,65]. Although the pharmacokinetics of Doxil® may be similar to our nanoformulation, with a half-life in the bloodstream greater than 24 h [64], its small size (~100 nm) [66] does not make it suitable for preventing drug entry into the DRG. However, it has been demonstrated optimal pharmacokinetic properties of a nanoformulation are reached with a size of 100 nm or less [67]. We have succeeded in synthesizing pegylated liposomes of a considerably larger size that comply with our premise of not penetrating the pores of the DRG whilst retaining all the advantages of a smaller nanoformulation, including good biodistribution, greater antitumor effect and the additional property of significantly reducing side effects related to PTX-induced peripheral neuropathy, which was our main goal. Similar nanoformulations which transport PTX such as Lipusu® have shown to reduce hypersensitivity reactions associated with Cremophor EL, which are mediated by increased histamine release and non-activation of the complement system [68], as well as bone marrow and heart toxicity [69]. However, its effect on PTX-induced peripheral neuropathy has not been described. Conversely, Abraxane® or nab-PTX, a nanoformulation based on human serum albumin with PTX, showed an increased risk of PTX-induced peripheral neuropathy compared to free PTX [70,71]. Consequently, the liposomal nanoformulations currently marketed do not solve or even aggravate the problem of peripheral neuropathy. It is therefore necessary to develop new nanoformulations optimized to avoid this serious side effect, like our MLV-PEG-PTX.

5. Conclusions

Two commercial cationic liposomes with different diameters based on the size of the EFs of the DRG were used in order to improve the pharmacological properties of PTX and to avoid peripheral neuropathy, one of the main side effects of this drug. Both MLV and SUV liposomes showed excellent biocompatibility with both human erythrocytes and cell lines and enhanced the antitumor effect of PTX, not only in cultured lung cancer cells, but also in lung CSCs and in MTS models. In addition, *in vivo* assays using mouse models with induced tumors also demonstrated that MLV-PEG-PTX and SUV-PEG-PTX can significantly reduce the tumor volume in comparison with free PTX. Interestingly, the distribution analysis detected a very low concentration of PTX in the DRG of mice using large liposomes (MLV-PEG-PTX) compared to smaller liposomes (SUV-PEG-PTX) and free PTX. These results were corroborated by pain behavioral tests in mice, supporting the hypothesis that the liposome size may be decisive to prevent the development of peripheral neuropathy. Therefore, our MLV liposomes could be a new option for chemotherapeutic treatment with PTX because, in addition to demonstrating numerous advantages such as biocompatibility, specificity for tumor cells, antitumor activity against CSCs and reduction of tumor volume *in vivo*, they could prevent the development of painful peripheral neuropathy, a property that has not been observed in previous studies using liposomes.

Funding source

All sources of funding should be acknowledged, and you should declare any extra funding you have received for academic research of this work. If there are none state 'there are none'.

Declaration of Competing Interest

The authors declare no conflict of interest.

Acknowledgments

The authors would like to thank technical assistance from the Centro de Instrumentación Científica (CIC) (University of Granada). This work was funded by the *Consejería de Salud de la Junta de Andalucía* (projects

P11-CTS-7649, PI-0102-2017 and P18-TP-3882) and by the CTS-107 Group. This work was also partially supported by a grant from the *Instituto de Salud Carlos III* (ISCIII) (Project PI19/01478) (FEDER).

Appendix A. Supplementary data

Supplementary material related to this article can be found, in the online version, at doi:https://doi.org/10.1016/j.biopha.2020.111059.

References

[1] F. Bray, J. Ferlay, I. Soerjomataram, R.L. Siegel, L.A. Torre, A. Jemal, Global cancer statistics 2018: GLOBOCAN estimates of incidence and mortality worldwide for 36 cancers in 185 countries, CA Cancer J. Clin. 68 (2018) 394–424, https://doi.org/10.3322/caac.21492.

[2] P. Goldstraw, J. Crowley, K. Chansky, D.J. Giroux, P.A. Groome, R. Rami-Porta, P. E. Postmus, V. Rusch, L. Sobin, C. International Association for the Study of Lung Cancer International Staging, I, Participating, the IASLC Lung Cancer Staging Project: proposals for the revision of the TNM stage groupings in the forthcoming (seventh) edition of the TNM Classification of malignant tumours, J. Thorac. Oncol. 2 (2007) 706–714, https://doi.org/10.1097/JTO.0b013e31812f3c1a.

[3] D.E. Midthun, Early detection of lung cancer, F1000Res 5 (2016), https://doi.org/10.12688/f1000research.7313.1.

[4] G. Alvarado-Luna, D. Morales-Espinosa, Treatment for small cell lung cancer, where are we now?-A review, Transl. Lung Cancer Res. 5 (2016) 26–38, https://doi.org/10.3978/j.issn.2218-6751.2016.01.13.

[5] F. Grossi, C. Gridelli, M. Aita, F. De Marinis, Identifying an optimum treatment strategy for patients with advanced non-small cell lung cancer, Crit. Rev. Oncol. Hematol. 67 (2008) 16–26, https://doi.org/10.1016/j.critrevonc.2007.12.002.

[6] P. Harper, G.M. Marx, Combined modality treatments in early non-small cell lung cancer, Lung Cancer 38 (2002) S23–25.

[7] G.V. Scagliotti, F. De Marinis, M. Rinaldi, L. Crino, C. Gridelli, S. Ricci, E. Matano, C. Boni, M. Marangolo, G. Failla, G. Altavilla, V. Adamo, A. Ceribelli, M. Clerici, F. Di Costanzo, L. Frontini, M. Tonato, P. Italian Lung Cancer, phase III randomized trial comparing three platinum-based doublets in advanced non-small-cell lung cancer, J. Clin. Oncol. 20 (2002) 4285–4291, https://doi.org/10.1200/JCO.2002.02.068.

[8] C. Hardin, E. Shum, A.P. Singh, R. Perez-Soler, H. Cheng, Emerging treatment using tubulin inhibitors in advanced non-small cell lung cancer, Expert Opin. Pharmacother. 18 (2017) 701–716, https://doi.org/10.1080/14656566.2017.1316374.

[9] M.A. Jordan, L. Wilson, Microtubules as a target for anticancer drugs, Nat. Rev. Cancer 4 (2004) 253–265, https://doi.org/10.1038/nrc1317.

[10] A.E. Prota, K. Bargsten, D. Zurwerra, J.J. Field, J.F. Diaz, K.H. Altmann, M. O. Steinmetz, Molecular mechanism of action of microtubule-stabilizing anticancer agents, Science 339 (2013) 587–590, https://doi.org/10.1126/science.1230582.

[11] M. Ranson, N. Davidson, M. Nicolson, S. Falk, J. Carmichael, P. Lopez, H. Anderson, N. Gustafson, A. Jeynes, G. Gallant, T. Washington, N. Thatcher, Randomized trial of paclitaxel plus supportive care versus supportive care for patients with advanced non-small-cell lung cancer, J. Natl. Cancer Inst. 92 (2000) 1074–1080.

[12] F. Leonessa, R. Clarke, ATP binding cassette transporters and drug resistance in breast cancer, Endocr. Relat. Cancer 10 (2003) 43–73.

[13] Z. Weiszhar, J. Czucz, C. Revesz, L. Rosivall, J. Szebeni, Z. Rozsnyay, Complement activation by polyethoxylated pharmaceutical surfactants: Cremophor-EL, Tween-80 and Tween-20, Eur. J. Pharm. Sci. 45 (2012) 492–498, https://doi.org/10.1016/j.ejps.2011.09.016.

[14] L. Jiang, L. Li, X. He, Q. Yi, B. He, J. Cao, W. Pan, Z. Gu, Overcoming drug-resistant lung cancer by paclitaxel loaded dual-functional liposomes with mitochondria targeting and pH-response, Biomaterials 52 (2015) 126–139, https://doi.org/10.1016/j.biomaterials.2015.02.004.

[15] E. Bernabeu, M. Cagel, E. Lagomarsino, M. Moretton, D.A. Chiappetta, Paclitaxel: What has been done and the challenges remain ahead, Int. J. Pharm. 526 (2017) 474–495, https://doi.org/10.1016/j.ijpharm.2017.05.016.

[16] K. He, M. Tang, Safety of novel liposomal drugs for cancer treatment: advances and prospects, Chem. Biol. Interact. 295 (2017) 13–19, https://doi.org/10.1016/j.cbi.2017.09.006.

[17] F.S. Mozar, E.H. Chowdhury, Impact of PEGylated nanoparticles on tumor targeted drug delivery, Curr. Pharm. Des. 24 (2018) 3283–3296, https://doi.org/10.2174/1381612824666180730161721.

[18] A.A. Argyriou, M. Koltzenburg, P. Polychronopoulos, S. Papapetropoulos, H. P. Kalofonos, Peripheral nerve damage associated with administration of taxanes in patients with cancer, Crit. Rev. Oncol. Hematol. 66 (2008) 218–228, https://doi.org/10.1016/j.critrevonc.2008.01.008.

[19] F. De Iuliis, L. Taglieri, G. Salerno, R. Lanza, S. Scarpa, Taxane induced neuropathy in patients affected by breast cancer: literature review, Crit. Rev. Oncol. Hematol. 96 (2015) 34–45, https://doi.org/10.1016/j.critrevonc.2015.04.011.

[20] P.M. Dougherty, J.P. Cata, J.V. Cordella, A. Burton, H.R. Weng, Taxol-induced sensory disturbance is characterized by preferential impairment of myelinated fiber function in cancer patients, Pain 109 (2004) 132–142, https://doi.org/10.1016/j.pain.2004.01.021.

[21] J.R. Brewer, G. Morrison, M.E. Dolan, G.F. Fleming, Chemotherapy-induced peripheral neuropathy: current status and progress, Gynecol. Oncol. 140 (2016) 176–183, https://doi.org/10.1016/j.ygyno.2015.11.011.

[22] H. Starobova, I. Vetter, Pathophysiology of chemotherapy-induced peripheral neuropathy, Front. Mol. Neurosci. 10 (2017) 174, https://doi.org/10.3389/fnmol.2017.00174.

[23] N.A. Duggett, L.A. Griffiths, S.J.L. Flatters, Paclitaxel-induced painful neuropathy is associated with changes in mitochondrial bioenergetics, glycolysis, and an energy deficit in dorsal root ganglia neurons, Pain 158 (2017) 1499–1508, https://doi.org/10.1097/j.pain.0000000000000939.

[24] C.M. Peters, J.M. Jimenez-Andrade, M.A. Kuskowski, J.R. Ghilardi, P.W. Mantyh, An evolving cellular pathology occurs in dorsal root ganglia, peripheral nerve and spinal cord following intravenous administration of paclitaxel in the rat, Brain Res. 1168 (2007) 46–59, https://doi.org/10.1016/j.brainres.2007.06.066.

[25] S.M. Jamieson, J. Liu, T. Hsu, B.C. Baguley, M.J. McKeage, Paclitaxel induces nucleolar enlargement in dorsal root ganglion neurons in vivo reducing oxaliplatin toxicity, Br. J. Cancer 88 (2003) 1942–1947, https://doi.org/10.1038/sj.bjc.6601012.

[26] R.W. Gregg, J.M. Molepo, V.J. Monpetit, N.Z. Mikael, D. Redmond, M. Gadia, D. J. Stewart, Cisplatin neurotoxicity: the relationship between dosage, time, and platinum concentration in neurologic tissues, and morphologic evidence of toxicity, J. Clin. Oncol. 10 (1992) 795–803, https://doi.org/10.1200/JCO.1992.10.5.795.

[27] W.H. Xiao, H. Zheng, F.Y. Zheng, R. Nuydens, T.F. Meert, G.J. Bennett, Mitochondrial abnormality in sensory, but not motor, axons in paclitaxel-evoked painful peripheral neuropathy in the rat, Neuroscience 199 (2011) 461–469, https://doi.org/10.1016/j.neuroscience.2011.10.010.

[28] J.M. Jimenez-Andrade, M.B. Herrera, J.R. Ghilardi, M. Vardanyan, O. K. Melemedjian, P.W. Mantyh, Vascularization of the dorsal root ganglia and peripheral nerve of the mouse: implications for chemical-induced peripheral sensory neuropathies, Mol. Pain 4 (2008) 10, https://doi.org/10.1186/1744-8069-4-10.

[29] M.C. Leiva, R. Ortiz, R. Contreras-Caceres, G. Perazzoli, I. Mayevych, J.M. Lopez-Romero, F. Sarabia, J.M. Baeyens, C. Melguizo, J. Prados, Tripalmitin nanoparticle formulations significantly enhance paclitaxel antitumor activity against breast and lung cancer cells in vitro, Sci. Rep. 7 (2017), 13506, https://doi.org/10.1038/s41598-017-13816-z.

[30] M. Li, E.A. Czyszczon, J.J. Reineke, Delineating intracellular pharmacokinetics of paclitaxel delivered by PLGA nanoparticles, Drug Deliv. Transl. Res. 3 (2013) 551–561, https://doi.org/10.1007/s13346-013-0162-y.

[31] M.A. Fernandez-Peralbo, F. Priego-Capote, M.D. Luque de Castro, A. Casado-Adam, A. Arjona-Sanchez, F.C. Munoz-Casares, LC-MS/MS quantitative analysis of paclitaxel and its major metabolites in serum, plasma and tissue from women with ovarian cancer after intraperitoneal chemotherapy, J. Pharm. Biomed. Anal. 91 (2014) 131–137, https://doi.org/10.1016/j.jpba.2013.12.028.

[32] J. Prados, C. Melguizo, A. Rama, R. Ortiz, H. Boulaiz, F. Rodriguez-Serrano, O. Caba, J.J. Rodriguez-Herva, J.L. Ramos, A. Aranega, Combined therapy using suicide gef gene and paclitaxel enhances growth inhibition of multicellular tumour spheroids of A-549 human lung cancer cells, Int. J. Oncol. 33 (2008) 121–127.

[33] J. Jimenez-Lopez, M.M. El-Hammadi, R. Ortiz, M.D. Cayero-Otero, L. Cabeza, G. Perazzoli, L. Martin-Banderas, J.M. Baeyens, J. Prados, C. Melguizo, A novel nanoformulation of PLGA with high non-ionic surfactant content improves in vitro and in vivo PTX activity against lung cancer, Pharmacol. Res. 141 (2019) 451–465, https://doi.org/10.1016/j.phrs.2019.01.013.

[34] E.J. Cobos, C.A. Nickerson, F. Gao, V. Chandran, I. Bravo-Caparros, R. Gonzalez-Cano, P. Riva, N.A. Andrews, A. Latremoliere, C.R. Seehus, G. Perazzoli, F.R. Nieto, N. Joller, M.W. Painter, C.H.E. Ma, T. Omura, E.J. Chesler, D.H. Geschwind, G. Coppola, M. Rangachari, C.J. Woolf, M. Costigan, Mechanistic differences in neuropathic pain modalities revealed by correlating behavior with global expression profiling, Cell Rep. 22 (2018) 1301–1312, https://doi.org/10.1016/j.celrep.2018.01.006.

[35] I. Bravo-Caparros, G. Perazzoli, S. Yeste, D. Cikes, J.M. Baeyens, E.J. Cobos, F. R. Nieto, Sigma-1 receptor inhibition reduces neuropathic pain induced by partial sciatic nerve transection in mice by opioid-dependent and -Independent mechanisms, Front. Pharmacol. 10 (2019) 613, https://doi.org/10.3389/fphar.2019.00613.

[36] J.A. Sparano, M. Wang, S. Martino, V. Jones, E.A. Perez, T. Saphner, A.C. Wolff, G. W. Sledge Jr., W.C. Wood, N.E. Davidson, Weekly paclitaxel in the adjuvant treatment of breast cancer, N. Engl. J. Med. 358 (2008) 1663–1671, https://doi.org/10.1056/NEJMoa0707056.

[37] T.B. Stage, T.K. Bergmann, D.L. Kroetz, Clinical pharmacokinetics of paclitaxel monotherapy: an updated literature review, Clin. Pharmacokinet. 57 (2018) 7–19, https://doi.org/10.1007/s40262-017-0563-z.

[38] H. Gelderblom, J. Verweij, K. Nooter, A. Sparreboom, E.L. Cremophor, The drawbacks and advantages of vehicle selection for drug formulation, Eur. J. Cancer 37 (2001) 1590–1598.

[39] A.J. ten Tije, J. Verweij, W.J. Loos, A. Sparreboom, Pharmacological effects of formulation vehicles : implications for cancer chemotherapy, Clin. Pharmacokinet. 42 (2003) 665–685, https://doi.org/10.2165/00003088-200342070-00005.

[40] N.R. Kuznetsova, C. Sevrin, D. Lespineux, N.V. Bovin, E.L. Vodovozova, T. Meszaros, J. Szebeni, C. Grandfils, Hemocompatibility of liposomes loaded with lipophilic prodrugs of methotrexate and melphalan in the lipid bilayer, J. Control. Release 160 (2012) 394–400, https://doi.org/10.1016/j.jconrel.2011.12.010.

[41] Y. Nie, L. Ji, H. Ding, L. Xie, L. Li, B. He, Y. Wu, Z. Gu, Cholesterol derivatives based charged liposomes for doxorubicin delivery: preparation, in vitro and in vivo

characterization, Theranostics 2 (2012) 1092–1103, https://doi.org/10.7150/thno.4949.
[42] S.S. Hong, J.Y. Choi, J.O. Kim, M.K. Lee, S.H. Kim, S.J. Lim, Development of paclitaxel-loaded liposomal nanocarrier stabilized by triglyceride incorporation, Int. J. Nanomed. 11 (2016) 4465–4477, https://doi.org/10.2147/IJN.S113723.
[43] Q. Zhang, J. Wang, H. Zhang, D. Liu, L. Ming, L. Liu, Y. Dong, B. Jian, D. Cai, The anticancer efficacy of paclitaxel liposomes modified with low-toxicity hydrophobic cell-penetrating peptides in breast cancer: an in vitro and in vivo evaluation, RSC Adv. 8 (2018) 24084–24093.
[44] H. Hua, N. Zhang, D. Liu, L. Song, T. Liu, S. Li, Y. Zhao, Multifunctional gold nanorods and docetaxel-encapsulated liposomes for combined thermo- and chemotherapy, Int. J. Nanomed. 12 (2017) 7869–7884, https://doi.org/10.2147/IJN.S143977.
[45] H.B. Ruttala, Y.T. Ko, Liposome encapsulated albumin-paclitaxel nanoparticle for enhanced antitumor efficacy, Pharm. Res. 32 (2015) 1002–1016, https://doi.org/10.1007/s11095-014-1512-2.
[46] C. Wang, S.B. Huang, M.C. Yang, Y.T. Lin, I.H. Chu, Y.N. Shen, Y.H. Chiu, S. H. Hung, L. Kang, Y.R. Hong, C.H. Chen, Combining paclitaxel with ABT-263 has a synergistic effect on paclitaxel resistant prostate cancer cells, PLoS One 10 (2015), e0120913, https://doi.org/10.1371/journal.pone.0120913.
[47] M. Heney, M. Alipour, D. Vergidis, A. Omri, C. Mugabe, J. Th'ng, Z. Suntres, Effectiveness of liposomal paclitaxel against MCF-7 breast cancer cells, Can. J. Physiol. Pharmacol. 88 (2010) 1172–1180, https://doi.org/10.1139/Y10-097.
[48] R.H. Wang, H.M. Cao, Z.J. Tian, B. Jin, Q. Wang, H. Ma, J. Wu, Efficacy of dual-functional liposomes containing paclitaxel for treatment of lung cancer, Oncol. Rep. 33 (2015) 783–791, https://doi.org/10.3892/or.2014.3644.
[49] S. Pereira, R. Egbu, G. Jannati, W.T. Al-Jamal, Docetaxel-loaded liposomes: the effect of lipid composition and purification on drug encapsulation and in vitro toxicity, Int. J. Pharm. 514 (2016) 150–159, https://doi.org/10.1016/j.ijpharm.2016.06.057.
[50] X. Zhang, Y. Lou, X. Zheng, H. Wang, J. Sun, Q. Dong, B. Han, Wnt blockers inhibit the proliferation of lung cancer stem cells, Drug Des. Devel. Ther. 9 (2015) 2399–2407, https://doi.org/10.2147/DDDT.S76602.
[51] C. Zhao, S. Setrerrahmane, H. Xu, Enrichment and characterization of cancer stem cells from a human non-small cell lung cancer cell line, Oncol. Rep. 34 (2015) 2126–2132, https://doi.org/10.3892/or.2015.4163.
[52] S. Luanpitpong, L. Wang, V. Castranova, Y. Rojanasakul, Induction of stem-like cells with malignant properties by chronic exposure of human lung epithelial cells to single-walled carbon nanotubes, Part. Fibre Toxicol. 11 (2014) 22, https://doi.org/10.1186/1743-8977-11-22.
[53] Q. Yang, T. Zhang, C. Wang, J. Jiao, J. Li, Y. Deng, Coencapsulation of epirubicin and metformin in PEGylated liposomes inhibits the recurrence of murine sarcoma S180 existing CD133+ cancer stem-like cells, Eur. J. Pharm. Biopharm. 88 (2014) 737–745, https://doi.org/10.1016/j.ejpb.2014.10.006.
[54] A. Furedi, K. Szebenyi, S. Toth, M. Cserepes, L. Hamori, V. Nagy, E. Karai, P. Vajdovich, T. Imre, P. Szabo, D. Szuts, J. Tovari, G. Szakacs, Pegylated liposomal formulation of doxorubicin overcomes drug resistance in a genetically engineered mouse model of breast cancer, J. Control. Release 261 (2017) 287–296, https://doi.org/10.1016/j.jconrel.2017.07.010.
[55] L. Zhao, Y. Ye, J. Li, Y.M. Wei, Preparation and the in-vivo evaluation of paclitaxel liposomes for lung targeting delivery in dogs, J. Pharm. Pharmacol. 63 (2011) 80–86, https://doi.org/10.1111/j.2042-7158.2010.01184.x.
[56] J. Wu, A. Lee, Y. Lu, R.J. Lee, Vascular targeting of doxorubicin using cationic liposomes, Int. J. Pharm. 337 (2007) 329–335.
[57] S.K. Adesina, A. Holly, G. Kramer-Marek, J. Capala, E.O. Akala, Polylactide-based paclitaxel-loaded nanoparticles fabricated by dispersion polymerization: characterization, evaluation in cancer cell lines, and preliminary biodistribution studies, J. Pharm. Sci. 103 (2014) 2546–2555, https://doi.org/10.1002/jps.24061.
[58] Z. Qi, L. Yin, Y. Xu, F. Wang, Pegylated liposomalpaclitaxel induces ovarian cancer cell apoptosis via TNFinduced ERK/AKT signaling pathway, Mol. Med. Rep. 17 (2018) 7497–7504, https://doi.org/10.3892/mmr.2018.8811.
[59] T. Yang, F.D. Cui, M.K. Choi, J.W. Cho, S.J. Chung, C.K. Shim, D.D. Kim, Enhanced solubility and stability of PEGylated liposomal paclitaxel: in vitro and in vivo evaluation, Int. J. Pharm. 338 (2007) 317–326, https://doi.org/10.1016/j.ijpharm.2007.02.011.
[60] J.M. Jacobs, R.M. Macfarlane, J.B. Cavanagh, Vascular leakage in the dorsal root ganglia of the rat, studied with horseradish peroxidase, J. Neurol. Sci. 29 (1976) 95–107, https://doi.org/10.1016/0022-510x(76)90083-6.
[61] K.M. Wozniak, J.J. Vornov, Y. Wu, Y. Liu, V.A. Carozzi, V. Rodriguez-Menendez, E. Ballarini, P. Alberti, E. Pozzi, S. Semperboni, B.M. Cook, B.A. Littlefield, K. Nomoto, K. Condon, S. Eckley, C. DesJardins, L. Wilson, M.A. Jordan, S. C. Feinstein, G. Cavaletti, M. Polydefkis, B.S. Slusher, Peripheral neuropathy induced by microtubule-targeted chemotherapies: insights into acute injury and long-term recovery, Cancer Res. 78 (2018) 817–829, https://doi.org/10.1158/0008-5472.CAN-17-1467.
[62] X. Zang, J.B. Lee, K. Deshpande, O.B. Garbuzenko, T. Minko, L. Kagan, Prevention of paclitaxel-induced neuropathy by formulation approach, J. Control. Release 303 (2019) 109–116, https://doi.org/10.1016/j.jconrel.2019.04.013.
[63] H. Zhang, Y.L.M. de Carvalho-Barbosa, A. Kavelaars, C.J. Heijnen, P.J. Albrecht, P. M. Dougherty, Dorsal root ganglion infiltration by macrophages contributes to paclitaxel chemotherapy-induced peripheral neuropathy, J. Pain 17 (2016) 775–786, https://doi.org/10.1016/j.jpain.2016.02.011.
[64] A. Gabizon, H. Shmeeda, Y. Barenholz, Pharmacokinetics of pegylated liposomal doxorubicin: review of animal and human studies, Clin. Pharmacokinet. 42 (2003) 419–436, https://doi.org/10.2165/00003088-200342050-00002.
[65] A.A. Gabizon, H. Shmeeda, S. Zalipsky, Pros and cons of the liposome platform in cancer drug targeting, J. Liposome Res. 16 (2006) 175–183, https://doi.org/10.1080/08982100600848769.
[66] H. Shen, Q. Gao, Q. Ye, S. Yang, Y. Wu, Q. Huang, X. Wang, Z. Sun, Peritumoral implantation of hydrogel-containing nanoparticles and losartan for enhanced nanoparticle penetration and antitumor effect, Int. J. Nanomed. 13 (2018) 7409–7426, https://doi.org/10.2147/IJN.S178585.
[67] A. Nagayasu, K. Uchiyama, H. Kiwada, The size of liposomes: a factor which affects their targeting efficiency to tumors and therapeutic activity of liposomal antitumor drugs, Adv. Drug Deliv. Rev. 10 (1999) 75–87, https://doi.org/10.1016/s0169-409x(99)00041-1.
[68] H. Wang, G. Cheng, Y. Du, L. Ye, W. Chen, L. Zhang, T. Wang, J. Tian, F. Fu, Hypersensitivity reaction studies of a polyethoxylated castor oil-free, liposome-based alternative paclitaxel formulation, Mol. Med. Rep. 7 (2013) 947–952, https://doi.org/10.3892/mmr.2013.1264.
[69] L. Ye, J. He, Z. Hu, Q. Dong, H. Wang, F. Fu, J. Tian, Antitumor effect and toxicity of Lipusu in rat ovarian cancer xenografts, Food Chem. Toxicol. 52 (2013) 200–206, https://doi.org/10.1016/j.fct.2012.11.004.
[70] L. Peng, Z. Bu, X. Ye, Y. Zhou, Q. Zhao, Incidence and risk of peripheral neuropathy with nab-paclitaxel in patients with cancer: a meta-analysis, Eur. J. Cancer Care (Engl.) 26 (2017) 1–11, https://doi.org/10.1111/ecc.12407.
[71] X. Guo, H. Sun, J. Dong, Y. Feng, H. Li, R. Zhuang, P. Wang, W. Cai, Y. Zhou, Does nab-paclitaxel have a higher incidence of peripheral neuropathy than solvent-based paclitaxel? Evidence from a systematic review and meta-analysis, Crit. Rev. Oncol. Hematol. 139 (2019) 16–23, https://doi.org/10.1016/j.critrevonc.2019.04.021.